Isotope dependence of radiative muon capture on the ^{58,60,62}Ni isotopes

T. P. Gorringe,[1] D. S. Armstrong,[2] C. Q. Chen,[3] E. Christy,[1] B. C. Doyle,[1] P. Gumplinger,[3] H. W. Fearing,[3] M. D. Hasinoff,[4] M. A. Kovash,[1] and D. H. Wright[3]

[1]*Department of Physics and Astronomy, University of Kentucky, Lexington, Kentucky 40506*

[2]*Department of Physics, College of William and Mary, Williamsburg, Virginia 23187*

[3]*TRIUMF, 4004 Wesbrook Mall, Vancouver, Canada V6T 2A3*

[4]*Department of Physics and Astronomy, University of British Columbia, Vancouver, British Columbia, Canada V6T 1Z1*

(Received 20 January 1998)

We report measurements of the photon rates and energy spectra from inclusive radiative muon capture on three nickel isotopes using a photon pair spectrometer at the TRIUMF cyclotron. The values of R_γ, the partial branching ratios of radiative muon capture for photon energies >57 MeV, for ^{58,60,62}Ni were found to be (in units of 10^{-5}) 1.48 ± 0.08, 1.39 ± 0.09, and 1.05 ± 0.06, assuming a Fermi-gas photon spectral shape. The results reveal a significant isotope effect in the nickel branching ratios and a simple empirical scaling of the present nickel and earlier nuclear R_γ data with neutron excess. Furthermore, the observed atomic mass and neutron excess dependence of the entire nuclear R_γ data set is well reproduced by a relativistic Fermi-gas calculation. The ability of the model to reproduce the variation of the R_γ data using the Goldberger-Treiman formula for g_p suggests there is no compelling reason to invoke a more exotic A-dependent renormalization of g_p. [S0556-2813(98)00409-9]

PACS number(s): 23.40.Hc, 11.40.Ha, 27.40.+z, 27.50.+e

I. INTRODUCTION

In semileptonic weak interactions the nucleon's axial and induced pseudoscalar form factors $F_A(q^2)$ and $F_P(q^2)$ and coupling constants $g_a=F_A(0)$ and $g_p=F_P(-0.88m_\mu^2)$ embody how the strong interaction dresses the nucleon's weak interaction. The approximate chiral symmetry of light quark interactions relates these weak form factors to the pion decay constant f_π and the pion-nucleon coupling constant $g_{\pi NN}$. It predicts that the induced pseudoscalar coupling is due to single pion exchange between the nucleonic current (to which it couples strongly) and the leptonic current (to which it couples weakly) and yields $g_p=6.5g_a$, a solid prediction of low-energy QCD [1,2]. The controversy concerning the experimental determination of the pseudoscalar coupling on the free proton, with ordinary muon capture on H_2 yielding $g_p=(7.0\pm1.3)g_a$ [3] and radiative muon capture on H_2 yielding $g_p=(9.8\pm0.7\pm0.3)g_a$ [4,5], has not (yet) seriously threatened the theoretical foundations of g_p.

When investigating bound nucleons rather than free nucleons, one normally uses the impulse approximation and replaces the free axial and pseudoscalar couplings g_a and g_p by effective axial and pseudoscalar couplings $\tilde{g}a$ and $\tilde{g}_p$. Differences between the free and effective couplings, due to the intrinsic differences between free and bound nucleon structure, to the effects of two- through A-body exchange currents, and to deficiencies in nuclear models, are of considerable interest. Theoretically, the renormalization of $\tilde{g}_a$ and $\tilde{g}_p$ via mechanisms including core polarization [6,7], mesonic currents and isobar excitations [8–10], and the partial restoration of chiral symmetry [11], have been explored. Experimentally, while a lot is known about the size and systematics of the effective axial coupling in nuclei [12,13], not much is known about the effective pseudoscalar coupling in nuclei.

It has been argued for many years that R_γ, the ratio of the rates of inclusive radiative muon capture and inclusive ordinary muon capture (for the experimentally observable photons >57 MeV), is relatively sensitive to the induced pseudoscalar coupling and relatively insensitive to the nuclear structure ingredients (see, for example, Ref. [14]). The argument for the pseudoscalar coupling sensitivity is based on the four-momentum transfer which is far from the pion-pole in ordinary muon capture (OMC) (making the effect of $\tilde{g}_p$ small) but can be close to the pion-pole in radiative muon capture (RMC) (making the effect of $\tilde{g}_p$ large). Detailed calculations [15–22] generally confirm that R_γ is sensitive to $\tilde{g}_p$, with R_γ roughly doubling when $\tilde{g}_p$ is changed from 0 to $6.5g_a$, and roughly doubling again when $\tilde{g}_p$ is changed from $6.5g_a$ to $13g_a$. The argument for the structure insensitivity is naively grounded in the partial cancellation of the nuclear matrix elements in the ratio of the RMC and OMC rates. However, because of the different role of the Gamow-Teller dipole and quadrupole matrix elements in RMC and OMC, the cancellation of the nuclear structure dependences in R_γ is incomplete.

Recent experimental work by groups at PSI [23,24] and TRIUMF [25–27] have yielded high-quality nuclear RMC data for light, medium, and heavy nuclei. These RMC rates, together with the corresponding OMC rates [28], reveal a simple systematic trend in the radiative muon capture partial branching ratio across the Segré chart: R_γ decreases as A increases.

A number of authors have used a variety of models [15–22] to calculate the dependence of R_γ on $\tilde{g}_p$ and thereby enable extraction of the effective pseudoscalar coupling from the nuclear RMC data. Using the available model calculations, Gmitrö and Truöl [29] and Döbeli *et al.* [23] pointed out that the systematic A dependence of the R_γ data maps

into a striking A dependence of the coupling $\tilde{g}_p$. These authors conjectured a substantial renormalization of the pseudoscalar coupling in the nuclear medium, with a large enhancement of $\tilde{g}_p$ for light nuclei and a large quenching of $\tilde{g}_p$ for heavy nuclei. Interestingly, Ericson *et al.* [8], based on the effects of pion exchange currents and Δ-hole excitations, had previously speculated that the pseudoscalar coupling might be substantially quenched in the nuclear medium.

However, there are good reasons to be rather cautious about interpreting the systematics of R_γ with A as evidence for the quenching of $\tilde{g}_p$ with increasing mass number. One reason for caution is that the small values of $\tilde{g}_p$ in heavy nuclei are obtained by applying the Fermi-gas model [17], whereas the large values of $\tilde{g}_p$ in light nuclei are obtained by applying the shell model [19–21]. Therefore the systematics of the extracted values of $\tilde{g}_p$ with the atomic mass may in fact reflect the systematics of the extracted value of $\tilde{g}_p$ with the nuclear model. It is evident that before one claims a decrease of R_γ with A as evidence of a decrease of $\tilde{g}_p$ with A, one must assess the alternative sources of systematic dependences of R_γ on A.

In fact, a number of effects (including variations in muon binding energy, proton Coulomb energy, and Pauli blocking) will lead to systematic variations of R_γ with A. These effects influence the phase space, and consequently the capture rates, for OMC and RMC. Since they influence the phase space and capture rates for OMC and RMC differently, they also influence R_γ. Whether such effects can or cannot account for the systematic behavior of the R_γ data is, therefore, the basic question.

Several theoretical papers have examined the behavior of R_γ with A including, most recently, the work of Fearing and Welsh [18]. Using a relativistic Fermi-gas model and the local density approximation they observed a number of systematic dependences of R_γ on atomic number Z, atomic mass A, and neutron excess $\alpha=(N-Z)/A$. For example, the increase in muon binding energy with Z yielded a decrease in R_γ with Z and the increase in Pauli blocking with α yielded a decrease in R_γ with α. Including such effects, Fearing and Welsh found reasonable agreement between the calculated and measured dependence of R_γ on A. However, the comparison of model and data made by Fearing and Welsh was somewhat limited by the published experimental data set. Specifically, the RMC data were from targets with strongly correlated values of A and α, rendering separation of the empirical atomic mass and neutron excess dependence of R_γ difficult.

This work is the first experimental study of the isotope effect in radiative muon capture. Our main goal is to more thoroughly explore the systematic behavior of R_γ and, in particular, to separate the empirical dependences on A and α of the nuclear R_γ data. Disentangling the dependence of R_γ on α and A will more critically test the various model calculations and assist in isolating the contribution of ''standard'' nuclear effects (such as Pauli blocking) and ''exotic'' nuclear effects (such as $\tilde{g}_p$ quenching). Specifically, we have measured partial branching ratios for the ^{58,60,62}Ni isotopes and, in essence, determined R_γ while substantially varying α and essentially fixing A. We chose the nickel isotopes because the OMC rates are measured [30], Fermi-gas calculations of the OMC and RMC rates are available [17,18], and a random phase approximation calculation of the OMC and RMC rates is underway [31].

The article is organized as follows. In Sec. II we briefly describe the RMC spectrometer at the TRIUMF cyclotron and provide details of the nickel targets, in Sec. III we describe the analysis of the photon rates and energy spectra, and in Sec. IV we discuss the extraction of the nickel isotope partial branching ratios R_γ and their comparison to earlier nuclear R_γ measurements and to the Fearing and Welsh Fermi-gas model calculation [18].

II. EXPERIMENTAL SETUP

The experiment was performed on the M9A muon beamline at the TRIUMF cyclotron. The μ^- production runs used a beam momentum of 63 MeV/c and an incident flux of $\sim 4\times 10^5$ s^{-1}. The π^- calibration runs used a beam momentum of 75 MeV/c and an incident flux of $\sim 8\times 10^4$ s^{-1}. The 63 MeV/c μ^- beam and the 75 MeV/c π^- beam yielded approximately the same stopping distribution and stopping fraction in the nickel targets.

The nickel targets were situated $\sim$15 cm downstream of four beam counters and $\sim$15 cm upstream of one veto counter. Each of the ^{58,60,62}Ni targets comprised approximately 55 g of Ni with chemical and isotopic purities of better than 99% (the targets were supplied by Oak Ridge National Laboratory). The ^{58,62}Ni targets were rolled rectangular plates of dimensions 5 cm$\times$5 cm$\times$0.2 cm mounted in a polystyrene support of mass $\sim$6 g. The ^{60}Ni target was nickel powder contained in a thin-windowed 7 g acrylic box of inner dimensions 5 cm$\times$5 cm$\times$0.3 cm and mounted in a polystyrene support of mass $\sim$6 g.

Photons from μ^- stops in the target were detected using the RMC spectrometer, which is described in detail in Ref. [32]. Photons emerging from the target were detected by conversion to e^+e^- pairs in a cylindrical lead sheet and tracking the e^+ and e^- in a cylindrical wire chamber and cylindrical drift chamber.

Data were collected for a total of 5.7×10^{10}, 7.8×10^{10}, and 7.8×10^{10} incident μ^- on the ^{58,60,62}Ni, respectively, and 4.6×10^9 and 4.8×10^9 incident μ^- on an empty nickel plate (i.e., polystyrene support) target and an empty nickel powder (i.e., polystyrene support and acrylic container) target. Data were also collected from radiative pion capture (RPC) in carbon and nickel targets for background, calibration, and normalization measurements.

III. DATA ANALYSIS

A. Event selection

To extract the nonprompt (i.e., muon-induced) photon events from the raw events we applied a series of cuts. Tracking cuts required a sufficiently large number of points and a sufficiently small χ^2 for the fits to the e^+ and e^- trajectories. Photon cuts imposed geometrical requirements on the e^+, e^- and photon trajectories, the most important being that the e^+ and e^- tracks coincide at the converter and that the photon originate from the target. In addition, a ''false photon'' cut removed events due to ran-

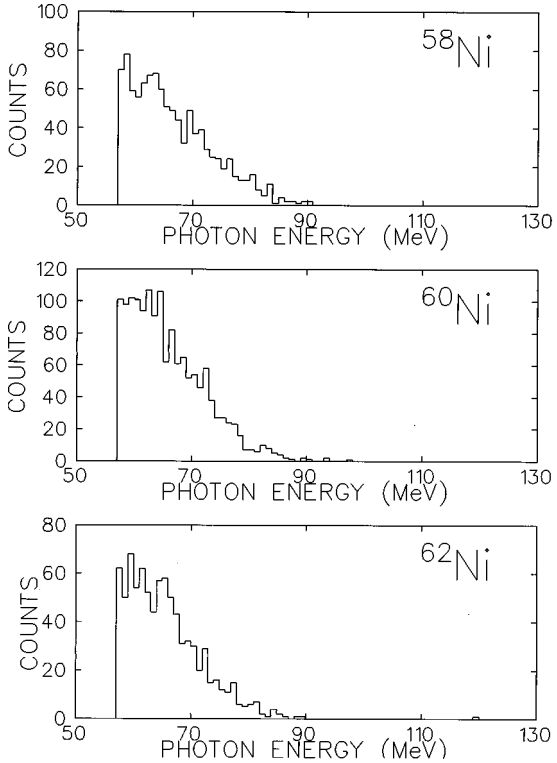

FIG. 1. The nonprompt photon energy spectra from the ^{58,60,62}Ni isotopes for $E>57$ MeV. The ^{58,60,62}Ni spectra contain 1038, 1492, and 848 photons in the energy region 57 to 100 MeV and 0, 1, and 1 photon(s) in the energy region 100 to 150 MeV, respectively.

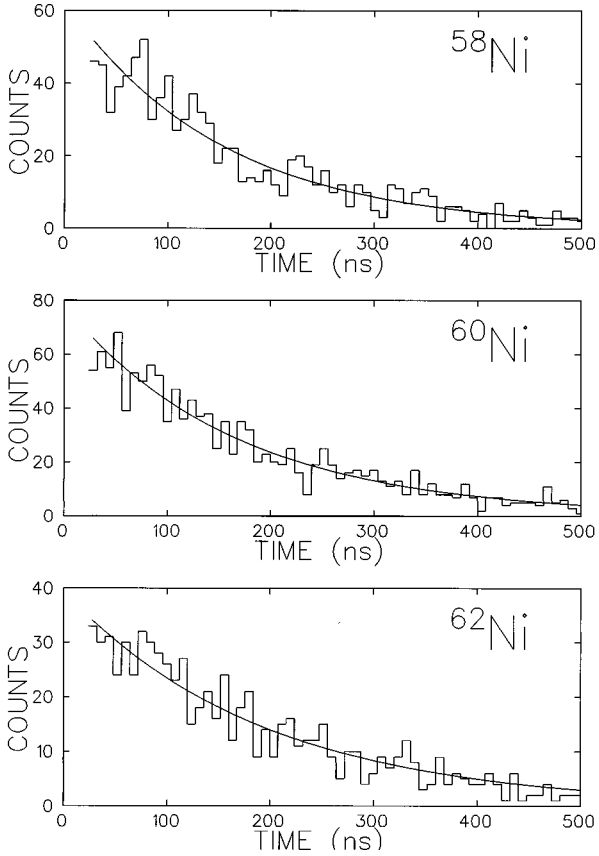

FIG. 2. The nonprompt photon time spectra from the ^{58,60,62}Ni isotopes. The histogram is the experimental data and the curve is the ''best fit'' exponential curve. The fit yielded lifetimes for the muonic ^{58,60,62}Ni isotopes of 154 ± 9, 169 ± 8, and 188 ± 12 ns, and background contributions of <1.4, 4.9 ± 0.7, and $<1.8\%$, respectively. The absence of counts in the time region 0 to 25 ns is due to the prompt cut.

dom combinations of Michel electron tracks, a cosmic cut removed events with coincident hits in the cosmic-ray counters, and a prompt cut removed events with coincident hits in the beam counters. More details on the cuts can be found in Refs. [5,27].

The nonprompt photon energy spectra and time spectra from the ^{58,60,62}Ni isotopes, after applying the cuts, are shown in Figs. 1 and 2, respectively. The ^{58,60,62}Ni energy spectra contain 1038, 1492, and 848 photons in the RMC energy window 57 to 100 MeV and 0, 1, and 1 photon(s) in the higher energy window 100 to 150 MeV, respectively [indicative of the small size of the (π^-,γ) and cosmic backgrounds]. The muonic ^{58,60,62}Ni lifetimes obtained from the ^{58,60,62}Ni time spectra were 154 ± 9, 169 ± 8, and 188 ± 12 ns, respectively (statistical uncertainties only), which are consistent with the lifetimes of 152.3 ± 2.4, 166.2 ± 2.6, and 193.4 ± 3.5 ns measured by Bobrov *et al.* [30].

B. Backgrounds

To obtain the number of nickel RMC events from the number of nonprompt photon events we subtracted several sources of background events. These were (i) radiative muon capture events from μ^- stops in the acrylic-polystyrene target holders, (ii) radiative pion capture events leaking through the prompt cut, (iii) $\mu^-\rightarrow e^-\nu\bar{\nu}\gamma$ bremmstrahlung events leaking from the kinematically allowed region below 53 MeV to the kinematically forbidden region above 53 MeV due to the small high-energy tail of the detector response function, and (iv) cosmic-ray events not rejected by the cosmic-ray cuts. These backgrounds were very important in the recent measurement of RMC on H_2 (branching ratio $\sim10^{-8}$) but rather small in this measurement of RMC on Ni (branching ratio $\sim10^{-5}$). More detailed discussions of these background sources can be found in Refs. [5] and [27].

The most carefully treated background was radiative muon capture on the polystyrene-acrylic target holders, since it was different for the ^{60}Ni (powder) target and the ^{58,62}Ni (plate) targets. From fits to the nickel time spectra we determined target-holder background contributions of $<1.3\%$, $(4.9\pm0.7)\%$, and $<1.8\%$ in the ^{58,60,62}Ni nonprompt photon spectra, while from the measured stops in ''full'' and ''empty'' target runs we determined target-holder background contributions of 0.3%, 3.8%, and 0.4% in the ^{58,60,62}Ni nonprompt photon spectra (using the previously measured RMC branching ratio for carbon [26]). Their consistency gave confidence in the target-holder background subtraction.

The other background sources were (i) similar for each isotope and (ii) very weak relative to the nickel signal. For the radiative pion capture background we set an upper limit of $<0.4\%$ via the relative counts in the 100–150 MeV region of the μ^-Ni and π^-Ni data. For the μ^--decay bremsstrahlung background we set an upper limit of $<0.2\%$ via Monte Carlo simulations and $\mu^+\rightarrow e^+\nu\bar{\nu}\gamma$ measurements of the high-energy tail (the μ^+ data were collected during our earlier measurement of RMC on H_2 [4,5]). For the cosmic-

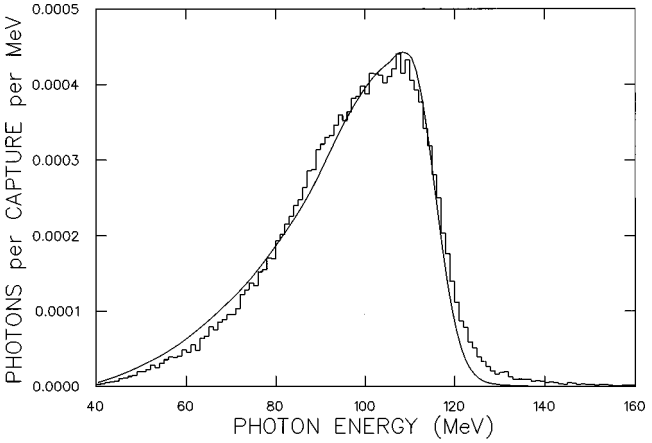

FIG. 3. Comparison of the measured (histogram) and simulated (curve) photon energy spectra from radiative pion capture on ^{12}C. The simulated spectrum was matched to the measured spectrum by multiplying by an overall normalization factor of $F=0.89$.

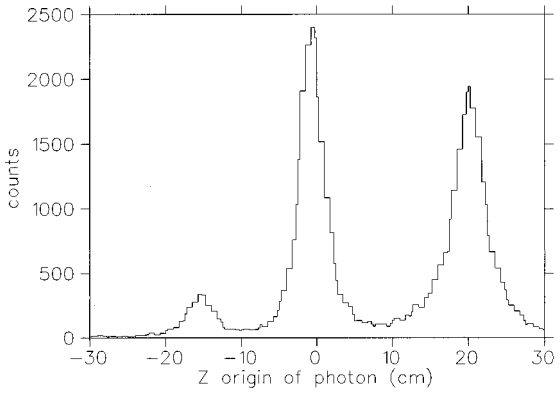

FIG. 4. The reconstructed photon origin along the beamline axis after the tracking cuts but before the photon cuts. The three peaks are due to the beam counters (left), the target assembly (center), and the veto counter (right).

ray backgrounds we obtained contributions of $(0.42\pm0.07)\%$, $(0.39\pm0.07)\%$, and $(0.76\pm0.13)\%$ for the ^{58,60,62}Ni isotopes via beam-off measurements.

After the subtraction of 4, 79, and 7 background photons, the unnormalized ^{58,60,62}Ni energy spectra contained 1034, 1413, and 841 signal photons in the energy range from 57 to 100 MeV.

C. Detector response function

To convert the number of RMC photons to a partial branching ratio of RMC photons we required the response function of the pair spectrometer. The response function $D(E,E')$ determines the probability of detecting a photon of true energy E with a measured energy E'.

The true (E) and measured (E') energy dependence of $D(E,E')$ was obtained via a computer simulation. The GEANT Monte Carlo package [34] was used to simulate the interactions of the initial photon and subsequent electrons in the target and detector, and the RMC data analysis package was used to analyze the simulated photon events in the same manner as the experimental photon events. The measured (i.e., E') photon energy spectra were simulated for true (i.e., E) monoenergetic photon energies of 50 to 140 MeV in 10 MeV steps. The results revealed a response function comprised of a Gaussian peak of full width at half maximum (FWHM) $\sim$12% with a relatively large low-energy tail and a relatively small high-energy tail. A simple analytical function, described in the Appendix, was fit to the simulated photon spectra and used to parametrize the E and E' dependence of $D(E,E')$. A similar parametrization was used in Ref. [27] although, due to the different triggers of this and the earlier work $(\overline{A+A'})\cdot\overline{B}\cdot C\cdot\geqslant 1D$ versus $\overline{(A+A')}\cdot\overline{B}\cdot C\cdot\geqslant 2D$, the functional form of $D(E,E')$ was somewhat different.

The absolute normalization of $D(E,E')$ was obtained from a comparison between a measurement and simulation of RPC on ^{12}C. The simulated spectrum was obtained using the analytical form of $D(E,E')$ in the Appendix and the measured RPC on ^{12}C photon yield and energy distribution of Perroud *et al.* [33]. Figure 3 shows a comparison of the measured and simulated RPC on ^{12}C spectra, in which the simulated spectrum was matched to the measured spectrum by multiplying by an overall normalization factor of $F=0.89\pm0.03$. The good agreement between the measured and simulated RPC on ^{12}C spectral shapes provided confidence in the calculation of the E and E' dependence of $D(E,E')$. The value of the factor F is consistent with the inefficiencies of the trigger scintillators and the wire chambers which are implicit in the measured spectrum but not in the simulated spectrum. The uncertainty in F is due to the uncertainty in the RPC on ^{12}C photon yield quoted in Ref. [33].

Several multiplicative correction factors were then applied to account for differences between the measurement of nonprompt radiative muon capture photons and prompt radiative pion capture photons. Three multiplicative factors accounted for the efficiencies of the false photon cut, cosmic cut, and prompt cut, which were applied to the RMC data but not to the RPC data (by efficiency we mean the cut's efficiency for passing valid RMC photon events, not the cut's efficiency for rejecting invalid RMC photon events). In the case of the prompt cut, values of $\epsilon_p=0.88$, 0.89, and 0.90 for ^{58,60,62}Ni were obtained based on the width of the prompt cut and the muon lifetime in the nickel isotopes. In the case of the false photon cut and the cosmic cut, values of $\epsilon_f=0.99$ and $\epsilon_c=0.89$–0.94 were obtained from their measured effects on the prompt (RPC) photon events in the nonprompt (RMC) photon data. The range in values of ϵ_c was due to different accelerator-related background rates leading to different cosmic-ray counter singles rates during the experiment. Finally, a correction factor $C_d=0.97$ accounted for

TABLE I. Fraction of muons stopping in the target assemblies for the ^{58,60,62}Ni runs. Column two gives the fraction of incident muons that stop in the nickel target material and the polystyrene-acrylic container. Column three gives the fraction of incident muons that stop in the nickel target material only. See text for details.

Target	Stop fraction for Ni and container	Stop fraction for Ni only	Stop fraction for container only
^{58}Ni	0.35	0.341 ± 0.003	0.005 ± 0.003
^{60}Ni	0.45	0.391 ± 0.013	0.061 ± 0.013
^{62}Ni	0.35	0.341 ± 0.003	0.005 ± 0.003

TABLE II. The nonprompt photon energy spectra after background subtraction $dN(E')/dE'$ for the ^{58,60,62}Ni isotopes.

E' (MeV)	$dN(E')/dE'$ for ^{58}Ni (counts per 2 MeV bin)	$dN(E')/dE'$ for ^{60}Ni (counts per 2 MeV bin)	$dN(E')/dE'$ for ^{62}Ni (counts per 2 MeV bin)
59.0	137.0	190.7	118.0
61.0	119.0	185.9	116.0
63.0	135.0	188.8	96.0
65.0	111.0	160.2	115.0
67.0	93.0	136.3	93.0
69.0	81.0	111.5	63.0
71.0	76.0	95.3	50.0
73.0	54.0	91.5	44.0
75.0	43.0	51.5	28.0
77.0	39.0	44.8	26.0
79.0	26.0	21.9	11.0
81.0	24.0	12.4	13.0
83.0	16.0	17.2	3.0
85.0	5.0	8.6	6.0
87.0	4.0	2.9	1.0
89.0	3.0	1.9	2.0
91.0	2.0	1.0	0.0
93.0	0.0	1.9	0.0
95.0	0.0	0.0	0.0
97.0	0.0	1.0	0.0
99.0	0.0	0.0	0.0

pion decays between the beam counters and the carbon target, a correction factor $C_t=0.94$ accounted for differences in the absorption and sizes of the carbon and nickel targets, and a correction factor $C_v=0.98$ accounted for the vetoing of photon events due to random hits in the A, A', and B trigger scintillators. The uncertainties in all the correction factors (ϵ_p, ϵ_f, ϵ_c, C_d, C_t, and C_v) were negligible in the final determination of the partial branching ratios R_γ.

D. Muon stop counting

Due to the small quantity of each nickel isotope, and therefore the small size of each nickel target, the measurement of the muon stopping fraction was critical. The problem is illustrated in Fig. 4, a plot of the reconstructed photon origin along the beamline axis. The peaks are due to photons from μ stops in the beam counters, target assembly, and veto counter.

To measure the muon stopping fraction, a prescaled coincidence of any two of the four beam scintillators generated beam-sample triggers in addition to the photon triggers. Offline the beam-sample data were analyzed to determine the muon, electron, and pion composition of the beam, and the stopping fraction of the incident muons in the target assemblies. The π, μ, and e identification used the amplitude and timing signals from the beam scintillators and indicated a 95% μ^-, 5% e^-, and 0.1% π^- beam composition. The muon stopping fraction determination used the amplitude and timing signals from the beam, veto, and inner trigger scintillators which completely enclose the target assembly. ''Full'' and ''empty'' target measurements yielded the fraction of muons stopped in the target material (powder or plate) and in the target container (polystyrene and/or acrylic). The various stopping fractions are listed in Table I—the quoted errors are based upon conservative estimates of the systematic uncertainties in the ''full less empty'' subtraction procedure.

IV. RESULTS

A. Extraction of R_γ

The true RMC photon spectrum $d\Lambda(E)/dE$ and the measured RMC photon spectrum $dN(E')/dE'$ are related through

$$\frac{dN(E')}{dE'}=N_\mu f_{\rm cap}\epsilon_p\epsilon_f\epsilon_c C_d C_t C_v F\int dE D(E,E')\frac{d\Lambda(E)}{dE}, \tag{1}$$

where E and E' are the true and measured photon energies, $D(E,E')$ is the Monte Carlo simulated detector response function, F is the overall normalization factor obtained from RPC on ^{12}C, the correction factors ϵ_p, ϵ_f, ϵ_c, C_d, C_t, and C_v account for the differences between RMC and RPC running, and N_μ and $f_{\rm cap}$ are the number of dead-time corrected μ stops in Ni, and the fraction of muons having stopped in nickel that undergo muon capture [30], respectively. Note that $d\Lambda(E)/dE$ is defined as the photon yield per muon capture. The measured RMC photon spectra $dN(E')/dE'$ are given in Table II while the numerical values of the remaining quantities in Eq. (1) are given in Table III. Tables II and III, along with the analytical form of the response function in the Appendix, should enable straightforward comparison of future model calculations of the true RMC photon spectrum $d\Lambda(E)/dE$ with the measured RMC energy spectrum $dN(E')/dE'$.

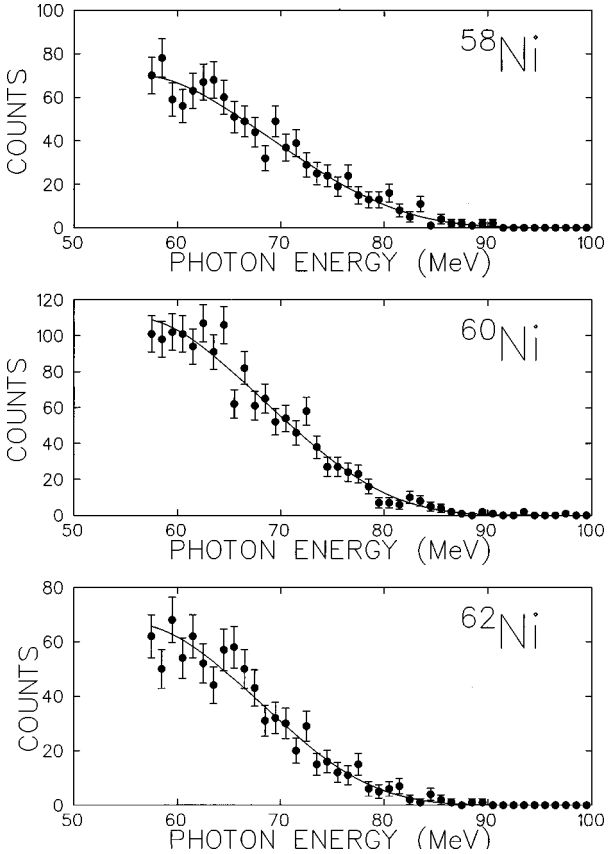

FIG. 5. Results of the fits of the Fermi-gas spectral shapes (the curves) to the measured spectral shapes (the histograms) for the ^{58,60,62}Ni isotopes, respectively. The theoretical curves have been convoluted with the detector response for comparison to the experimental data.

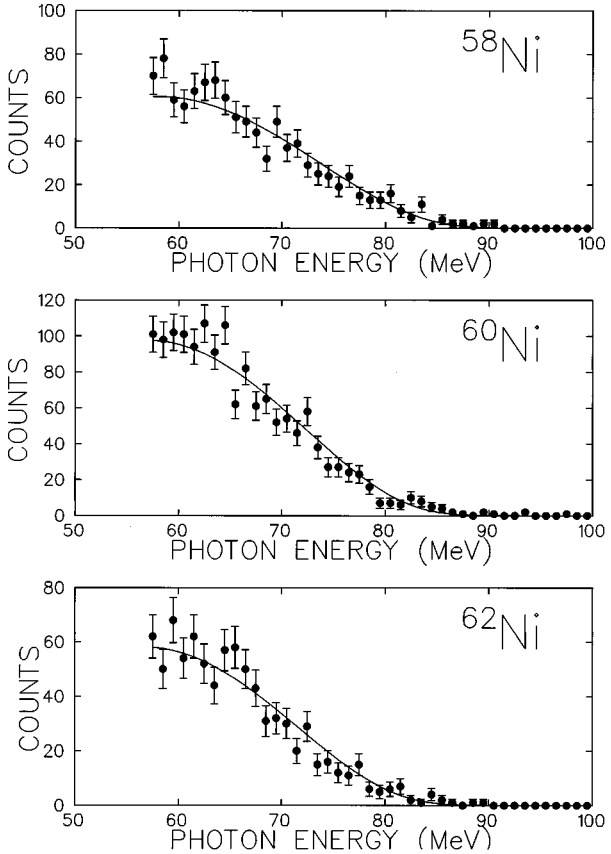

FIG. 6. Results of the fits of the closure approximation spectral shapes (the curves) to the measured spectral shapes (the histograms) for the ^{58,60,62}Ni isotopes, respectively. The theoretical curves have been convoluted with the detector response for comparison to the experimental data.

To determine the radiative muon capture partial branching ratio for true photon energies above 57 MeV

$$R_\gamma = \int_{57} dE \frac{d\Lambda(E)}{dE} \tag{2}$$

the function of $d\Lambda(E)/dE$ in Eq. (1) was varied to fit to the measurements of $dN(E')/dE'$ in Table II. The resulting ''best fit'' $d\Lambda(E)/dE$ then determines the best fit R_γ. Clearly, the method requires a conjecture or hypothesis for the true energy dependence of $d\Lambda(E)/dE$; we used both a Fermi gas spectral shape and a closure approximation spectral shape.

In the first approach we used the Fermi gas calculation of Fearing and Welsh [18]. This is a relativistic calculation using the local density approximation and realistic matter distributions, which is discussed in Sec. IV C. In the minimization procedure the energy dependence of $d\Lambda(E)/dE$ was fixed by the model, and the overall normalization of $d\Lambda(E)/dE$ was extracted from the best fit. The best fits of $d\Lambda(E)/dE$ to $(dNE')/dE'$ for the ^{58,60,62}Ni isotopes are shown in Fig. 5. They show good agreement between the spectral shapes of the data and the model with $\chi^2_{\rm pdf}$ values of 0.8, 1.0, and 0.9 for ^{58,60,62}Ni, respectively. The resulting values of the partial branching ratio R_γ for ^{58,60,62}Ni are 1.48 ± 0.08, 1.39 ± 0.09, and 1.05 ± 0.06 (in units of 10^{-5}). The quoted errors include both the statistical and systematic uncertainties, with the dominant systematic uncertainties coming from the overall normalization and the μ-stop counting.

In the second approach we used the closure approximation discussed, for example, in Ref. [17]. It is derived from the assumptions that (i) the muon radiates the photon and (ii) muon capture occurs to a single nuclear excitation energy. It yields

$$\frac{d\Lambda(E)}{dE} \propto (1-2x+2x^2)x(1-x)^2, \tag{3}$$

where x is the ratio of the photon energy to the end-point energy E/k_m. While the above assumptions are quite unreal-

TABLE III. The number of dead-time corrected muon stops (N_μ), the fraction of muon captures per muon stop ($f_{\rm cap}$), and the various correction factors (see text) ϵ_p, ϵ_f, ϵ_c, C_d, C_t, and C_v, for the ^{58,60,62}Ni measurements.

Target	N_μ ($\times 10^{10}$)	$f_{\rm cap}$	ϵ_p	ϵ_f	ϵ_c	C_d	C_t	C_v
^{58}Ni	1.79	0.931	0.88	0.99	0.94	0.97	0.94	0.98
^{60}Ni	2.85	0.924	0.89	0.99	0.89	0.97	0.94	0.98
^{62}Ni	2.36	0.912	0.90	0.99	0.89	0.97	0.94	0.98

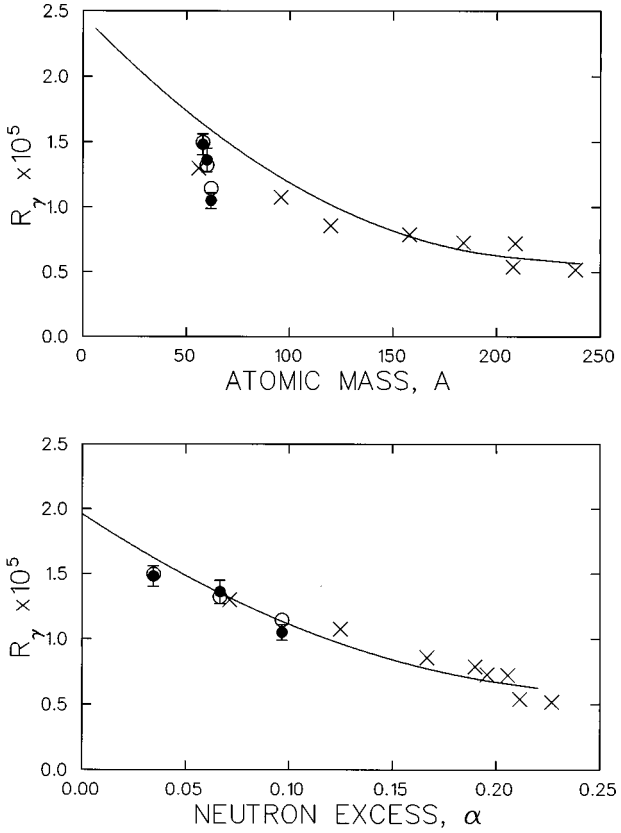

FIG. 7. The partial branching ratio R_γ versus atomic mass A (top) and neutron excess $\alpha=(N-Z)/A$ (bottom) for the current ^{58,60,62}Ni R_γ data (solid circles with error bars) and the Fermi-gas model of Fearing and Welsh (open circles for the ^{58,60,62}Ni values and crosses for the other values). The solid curves are least-square fits to the A and α dependences of the earlier nuclear R_γ data.

istic, Eq. (3) is a convenient form that often empirically fits the RMC spectral shapes rather well. In the minimization procedure both the overall normalization and the parameter k_m were varied to obtain the best fit. The best fits of $d\Lambda(E)/dE$ to $dN(E')/dE'$ for the ^{58,60,62}Ni isotopes are shown in Fig. 6. The $\chi^2_{\rm pdf}$ of 1.8, 2.0, and 1.3 for ^{58,60,62}Ni indicate poorer agreement between the data and model for the closure approximation spectral shapes than the Fermi gas spectral shapes; the closure approximation either overestimated the higher-energy photon yield, underestimated the lower-energy photon yield, or both. The resulting values of the partial branching ratio R_γ and the parameter k_m for ^{58,60,62}Ni are 1.39 ± 0.10, 1.36 ± 0.11, and 1.01 ± 0.07 (in units of 10^{-5}) and 92 ± 2, 90 ± 2, and 89 ± 2 MeV, respectively. The quoted errors include both the statistical and systematic uncertainties, with the dominant systematic uncertainties coming from the overall normalization, μ-stop counting, and the correlation between R_γ and k_m.

TABLE IV. Summary of the values of R_γ extracted using the Fermi gas spectral shapes and closure approximation spectral shapes for the ^{58,60,62}Ni isotopes.

Nickel isotope	$\alpha=(N-Z)/A$	R_γ Fermi gas spectral shape $\times10^{-5}$	R_γ closure approx. spectral shape $\times10^{-5}$
58	0.034	1.48 ± 0.08	1.39 ± 0.10
60	0.067	1.39 ± 0.09	1.36 ± 0.11
62	0.097	1.05 ± 0.06	1.01 ± 0.07

The results obtained with the Fermi-gas and closure approximation spectral shapes reveal a slight model dependence to R_γ (the better $\chi^2_{\rm pdf}$ of the Fermi-gas fits compared to the closure approximation fits favoring the former over the latter). However, the subsequent conclusions are not affected by this model dependence.

Table IV summarizes the values of R_γ for the ^{58,60,62}Ni isotopes extracted with both the Fermi-gas and closure approximation spectral shapes. Our most basic result is the significant isotope effect in the partial branching ratios for radiative muon capture on ^{58,60,62}Ni. The ratio of the values of R_γ for the heaviest (^{62}Ni) and lightest (^{58}Ni) isotopes are 0.71 ± 0.03 using the Fermi-gas spectral shape and 0.73 ± 0.04 using the closure approximation spectral shape. These ratios are rather accurately determined since many of the systematic uncertainties associated with the μ^--stop counting, overall normalization, energy calibration, and background subtraction cancel out (the ^{58}Ni and ^{62}Ni targets were fabricated identically).

B. Comparison to earlier R_γ data

Figure 7 shows the branching ratio R_γ for the nickel data plotted versus both atomic mass A and neutron excess α (the values of R_γ extracted using the Fermi-gas spectral shape are shown rather than the closure approximation spectral shape due to the better $\chi^2_{\rm pdf}$). For comparison we have overlayed curves embodying the A and α dependence of the earlier nuclear R_γ data. The curves are least squares fits of quadratic equations in either A or α to the data of Refs. [23–27]. The fits versus A and α of the earlier data yielded $\chi^2_{\rm pdf}$ of 1.56 and 1.28, respectively, indicating their good representation of the general trends of the experimental data.

What do the Fig. 7 comparisons of the α/A dependences of the earlier nuclear and current nickel data indicate? First, the plot versus atomic mass reveals the R_γ data set is not a smoothly decreasing function of A (i.e., our nickel data and the earlier nuclear data do not coincide in this plot). Secondly, the plot versus neutron excess reveals the R_γ data set is a smoothly decreasing function of α (i.e., our nickel data and the earlier nuclear data do coincide on this plot). Figure 7 therefore indicates that atomic mass-dependent effects are insufficient, and neutron-excess-dependent effects are critical, in understanding the systematics of the R_γ data set. (Of course it would be naive to believe a single parameter could completely determine R_γ, but the overall trend of R_γ with α is quite compelling.) In summary, without reference to nuclear models, the observation of a simple scaling of the R_γ data set with α but not A, and the resulting inferences concerning α- and A-dependent effects, is a basic result of this experimental work.

An earlier hint of the empirical scaling of the nuclear R_γ data being with neutron excess rather than atomic mass was the ^{27}Al and ^{28}Si R_γ data of Armstrong *et al.* [27]. The measured radiative muon capture partial branching ratios for ^{27}Al and ^{28}Si are 1.43 ± 0.13 and 1.93 ± 0.18, respectively (in units of 10^{-5}). As with the nickel data, the ^{27}Al and ^{28}Si

data are consistent with the overall α dependence, but inconsistent with the overall A dependence, of the nuclear R_γ data set. The difference between, and the significance of, the ^{27}Al and ^{28}Si results was discussed in Ref. [27].

C. Comparison to the Fermi-gas model

There exist two calculations of the atomic mass and neutron excess dependence of R_γ over a broad range of A and α. They are the calculations of Christillin, Rosa-Clot, and Servadio (CRS) in Ref. [17] and of Fearing and Welsh (FW) in Ref. [18]. Both the CRS and FW calculations use the Fermi-gas model and the local density approximation. However, while the FW model is a relativistic calculation employing a realistic nuclear matter distribution, the CRS model is a nonrelativistic calculation employing a uniform nuclear matter distribution. Essentially, the CRS calculation is an earlier simplified version of the FW calculation. Therefore, we compare the nuclear R_γ data set to the latter not the former.

The FW model results were taken from either Ref. [18] or, in the specific case of the nickel isotopes, calculated for the purpose of this manuscript by H.W.F. In both cases the muon 1S binding energies ($E_{\mu B}$) were taken from Ford and Willis [37] while the μ-atom 1S probability distributions ($|\phi_{1S}(r)|^2$) were obtained from nonrelativistic wave function solutions of a Fermi nuclear charge density. Two-parameter Fermi distributions were used for the nuclear matter distributions with the nuclear radii and skin thicknesses taken from either Ref. [35] or Ref. [36]. The proton Coulomb energies (E_C) were determined from the energy difference of spheres of charges Z and $Z-1$ and the isospin symmetry energies (ΔE) were determined by requiring the agreement of the experimental and model nuclear mass differences. All calculations used $g_v=1$, $g_a=-1.25$, $g_m=3.71$, and the assumption that the corresponding form factors were independent of the four-momentum transfer squared. All calculations used an assumed pion-pole dominance for the four-momentum transfer squared dependence of the induced pseudoscalar form factor. Thus $\tilde{g}_p$ was given by the standard Goldberger-Treiman formula, which in the nuclear medium depends linearly on the effective mass, with the value $g_p=6.5g_a$ for the free nucleon. The absence of second class currents was assumed, i.e., $g_s=g_t=0$. For further details on the model calculation and the input parameters see Ref. [18].

Figure 7 shows R_γ versus α and A for both the experimental data (nickel data and earlier data) and the FW model calculation. Since the FW calculation is only applicable to medium-heavy nuclei, the FW results are only graphed for $Z>20$ nuclei. Since the FW calculations of R_γ universally overestimate the experimental values of R_γ, the calculated values have been universally multiplied by a factor of 0.36 (i.e., only the relative values of R_γ for the model calculations are significant). The new R_γ results from the FW model calculations for the ^{58,60,62}Ni isotopes were 4.20, 3.71, and 3.27, respectively (in units of 10^{-5} and before multiplication by 0.36). Figure 7 clearly shows the overall consistency of the measured and calculated values of R_γ when plotted versus neutron excess. In particular, the experimental and theoretical isotope dependences for the Ni R_γ data are in good agreement. For example, the ratio of R_γ between the ^{62}Ni and ^{58}Ni isotopes is 0.78 for the model calculation compared to 0.71 ± 0.03 (Fermi-gas spectral shape) and 0.73 ± 0.04 (closure approximation spectral shape) for the experimental data. As a consequence of the significant nickel isotope effect, the measured and calculated Ni data points lie on the α-dependence curve, but below the A-dependence curve, of the earlier nuclear data.

The addition of the nickel isotope R_γ data to the earlier nuclear R_γ data enables a better separation of the A and α dependence of R_γ and a better test of the FW model calculations of R_γ. The ability of the FW model to reproduce the variation of the R_γ data using the Goldberger-Treiman formula for $\tilde{g}_p$ suggests no reason to invoke a more exotic large-scale A-dependent modification of $\tilde{g}_p$. In the FW model the effective pseudoscalar coupling is proportional to the effective nucleon mass, and consequently, to first approximation, $\tilde{g}_p$ is simply reduced by a constant factor of $m^*/m\approx0.67$ from the GT value. Even in a more refined approximation, cf. the discussion of option 8 in Ref. [18], this nucleon mass effect is nearly A independent. It is somewhat a matter of semantics whether one calls this effect ''quenching,'' but our view is that the standard one-pion exchange picture on which the Goldberger-Treiman relation is based, is sufficient to describe the data. Thus there is no evidence for the more complicated non-one-pion exchange mechanisms which have been suggested to explain a supposed A dependence of $\tilde{g}_p$. Rather, we believe the evidence for a large enhancement of $\tilde{g}_p$ for light nuclei and a large quenching of $\tilde{g}_p$ for heavy nuclei (see Refs. [23] and [29]) is more likely a result of the different systematics of the various models used for the different nuclei. For example, the large values of $\tilde{g}_p$ were extracted from shell model calculations for light nuclei [19–21] while the small values of $\tilde{g}_p$ were extracted from Fermi-gas model calculations of heavy nuclei [17]. Since the Fermi-gas model does not give the correct overall scale of the nuclear matrix elements, the A-independent part of $\tilde{g}_p$, which effects this scale, cannot be determined. Hence comparisons of absolute values of $\tilde{g}_p$ between the shell model calculations for lighter nuclei and Fermi-gas model calculations for heavier nuclei are likely misleading. Lastly, the absence of any large-scale A-dependent renormalization of the induced pseudoscalar coupling is in general agreement with the various determinations of $\tilde{g}_p$ from OMC on light nuclei. The values of $\tilde{g}_p$ from OMC on ^{12}C [38–41], ^{16}O [42–44], and ^{23}Na [45,46] are universally consistent with the Goldberger-Treiman estimate of the free proton value of the induced pseudoscalar coupling $g_p=6.5g_a$ (an exception is the lower value of $\tilde{g}_p$ from OMC on ^{28}Si [47–49]).

The physical origins of the α and A dependence of R_γ were addressed in detail in Ref. [18]. A number of effects in the FW model calculation, including muon binding energy, proton Coulomb energy, isospin symmetry energy, and Pauli blocking lead to Z-, A-, and α-dependent systematic variations in R_γ (these effects alter the reaction Q value, available phase space, and consequently R_γ). Interestingly, the Z or A dependences introduced by the muon binding energy, proton Coulomb energy, and isospin symmetry energy while individually are quite large, together are quite small (the de-

crease in R_γ with A due to the first and third effects is largely canceled by the increase of R_γ with A due to the second effect). However, the increasing Pauli blocking with increasing neutron excess yields a decreasing R_γ with increasing α that is clearly exhibited in the final results of the FW calculation of R_γ versus α. The model indicates that Pauli blocking is an important source for the α dependence of the R_γ data.

Of course the Fermi gas model has deficiencies, for example, omitting the influences of collective motion and giant resonances that are important ingredients in muon capture (for a thorough discussion see the comprehensive article of Mukhopadhyay [14]). Therefore we cannot exclude the possibility that the deficiencies in the FW calculations could lead to accidental agreement with the R_γ data. A more sophisticated theoretical study of the A and α dependence of R_γ is, therefore, warranted and welcomed. New theoretical investigations of ordinary and radiative muon capture using the random phase approximation are currently underway [31].

V. SUMMARY

In summary, using the RMC spectrometer at the TRIUMF cyclotron we have measured the photon rates and energy spectra following radiative muon capture on the ^{58,60,62}Ni isotopes. The values of the partial branching ratios ($E>57$ MeV) for radiative muon capture on ^{58,60,62}Ni were found to be (in units of 10^{-5}) 1.48 ± 0.08, 1.39 ± 0.09, and 1.05 ± 0.06 assuming a Fermi-gas photon spectral shape and 1.39 ± 0.10, 1.36 ± 0.11, and 1.01 ± 0.07 assuming a closure approximation photon spectral shape. The nickel results demonstrate a significant isotope effect and a comparison of the current nickel R_γ data and earlier nuclear R_γ data suggests a simple scaling with neutron excess but not with atomic mass.

In addition, the α and A dependence of the current nickel R_γ data and earlier nuclear R_γ data is well reproduced by the Fermi-gas model calculations of Ref. [18]. Since the standard Goldberger-Treiman formula for $\tilde{g}_p$, modified only by its dependence on effective mass, seems sufficient to yield agreement with the data, we believe there is no compelling evidence for a more exotic A-dependent renormalization of $\tilde{g}_p$. This is generally consistent with the various determinations of $\tilde{g}_p$ from OMC on light nuclei.

ACKNOWLEDGMENTS

We would like to thank the staff of the TRIUMF laboratory for the operation of the cyclotron and the M9A separator and the maintenance of the RMC spectrometer. We would also like to thank Dr. Renée Poutissou for assistance with the data acquisition, Dr. John Macdonald for assistance with the M9A beamline, and Drs. Rudolf Eramzhyan, Volodya Kuz'min, Jean-Michel Poutissou, and Tanya Tetereva for many enlightening discussions. We would like to acknowledge both the National Science Foundation (United States) and the Natural Sciences and Engineering Research Council (Canada) for their financial assistance.

TABLE V. The coefficients a_0, a_1, a_2, and a_3 governing the energy dependence of the various parameters α, A, E_0, σ_0, and σ_2 of the response function of the pair spectrometer.

	a_0	a_1	a_2	a_3
α	56.1	62.5	-0.826	0.0
A	9.41×10^{-4}	2.61×10^{-3}	-0.270×10^{-2}	0.835×10^{-3}
E_0	54.5	57.7	-0.315	0.0
σ_0	2.03	10.4	1.25	-0.428
σ_2	0.786	0.508	0.425	-0.164

APPENDIX: DETECTOR RESPONSE FUNCTION $D(E,E')$

The response function of the pair spectrometer, i.e., the probability of detecting a photon of true energy E with a measured energy E', was obtained from a Monte Carlo simulation based on the GEANT computer program [34]. In the energy range $E=50$–150 MeV the response function $D(E,E')$ revealed a central peak with a relatively large low-energy tail and a relatively small high-energy tail. To conveniently parametrize its energy dependence we used a Gaussian peak with a logarithmically varying low-energy tail and an exponentially varying high-energy tail

$$D(E,E')=\beta\ln(x)/x \quad \text{for } E'\leqslant(E_0-\sigma_0), \tag{A1}$$

$$D(E,E')=Ae^{-(E'-E_0)^2/2\sigma_0^2} \quad \text{for } (E_0-\sigma_0)<E'<(E_0+\sigma_0^2/\sigma_2), \tag{A2}$$

$$D(E,E')=Ae^{-(E'-E_0)/2\sigma_2} \quad \text{for } E'\geqslant(E_0+\sigma_0^2/\sigma_2). \tag{A3}$$

The quantity β is used to match the functions in Eqs. (A1) and (A2) at $E'=E_0-\sigma_0$ and the quantity x is given by

$$x=\frac{(\alpha-E')}{(\alpha-37\ \text{MeV})}. \tag{A4}$$

According to Eqs. (A1)–(A3) the energy dependence of the response function is governed by the energy dependence of the parameters A, E_0, and σ_0 of the Gaussian peak, α of the low-energy tail, and σ_2 of the high-energy tail. The energy dependence of α, A, E_0, σ_0, and σ_2 were themselves parametrized by third-order polynomials, for example,

$$\alpha=a_0+a_1y+a_2y^2+a_3y^3, \tag{A5}$$

where $y=(E'-60\ \text{MeV})/60\ \text{MeV}$. The coefficients a_i for the parameters α, A, e_0, σ_0, and σ_2 are listed in Table V. These details are provided so that future theoretical spectra can be convoluted with the detector response function and compared to the data.

[1] M. L. Goldberger and S. B. Treiman, Phys. Rev. **110**, 1178 (1958).
[2] V. Bernard, N. Kaiser, and U-G. Meißner, Phys. Rev. Lett. **69**, 1877 (1992).
[3] G. Bardin, J. Duclos, A. Magnon, J. Martino, A. Richter, E. Zavattini, A. Bertin, M. Piccinini, A. Vitale, and D. Measday, Nucl. Phys. **A352**, 365 (1981).
[4] G. Jonkmans *et al.*, Phys. Rev. Lett. **77**, 4512 (1996).
[5] D. H. Wright *et al.*, Phys. Rev. C **57**, 373 (1998).
[6] I. Towner and F. Khanna, Nucl. Phys. **A399**, 334 (1983).
[7] A. Arima *et al.*, Adv. Nucl. Phys. **18**, 1 (1987).
[8] M. Ericson, A. Figureau, and C. Thévenet, Phys. Lett. **45B**, 19 (1973).
[9] J. Delorme, M. Ericson, A. Figureau, and C. Thévenet, Ann. Phys. (N.Y.) **102**, 273 (1976).
[10] J. Delorme and M. Ericson, Phys. Rev. C **49**, 1763 (1994).
[11] M. Rho, Annu. Rev. Nucl. Part. Sci. **34**, 531 (1984).
[12] D. Wilkinson, Phys. Rev. C **7**, 930 (1973); Nucl. Phys. **A209**, 470 (1973); **A225**, 365 (1974).
[13] B. A. Brown and B. H. Wildenthal, At. Data Nucl. Data Tables **33**, 347 (1985); Phys. Rev. C **28**, 2397 (1983); Annu. Rev. Nucl. Part. Sci. **38**, 29 (1988).
[14] N. Mukhopadhyay, Phys. Rep., Phys. Lett. **30C**, 1 (1977).
[15] P. Christillin, Nucl. Phys. **A362**, 391 (1981).
[16] P. Christillin and M. Gmitrö, Phys. Lett. **150B**, 50 (1985).
[17] P. Christillin, M. Rosa-Clot, and S. Servadio, Nucl. Phys. **A345**, 331 (1980).
[18] H. W. Fearing and M. S. Welsh, Phys. Rev. C **46**, 2077 (1992).
[19] M. Gmitrö, A. A. Ovchinnikova, and T. V. Tetereva, Nucl. Phys. **A453**, 685 (1986).
[20] M. Gmitrö, S. S. Kamalov, and A. A. Ovchinnikova, Nucl. Phys. **A468**, 404 (1987).
[21] M. Gmitrö, S. S. Kamalov, F. Simkovic, and A. A. Ovchinnikova, Nucl. Phys. **A507**, 707 (1990).
[22] F. Roig and J. Navarro, Phys. Lett. B **236**, 393 (1990).
[23] M. Döbeli, M. Doser, L. van Elmbt, M. W. Schaad, P. Truöl, A. Bay, J. P. Perroud, J. Imazato, and T. Ishikawa, Phys. Rev. C **37**, 1633 (1988).
[24] A. Frischknecht, M. Döbeli, W. Stehling, G. Strassner, P. Truöl, J. C. Alder, C. Joseph, J. F. Loude, J. P. Perroud, D. Ruegger, M. T. Tran, and H. Panke, Phys. Rev. C **38**, 1996 (1988).
[25] D. S. Armstrong *et al.*, Phys. Rev. C **40**, R1100 (1989).
[26] D. S. Armstrong *et al.*, Phys. Rev. C **43**, 1425 (1991).
[27] D. S. Armstrong *et al.*, Phys. Rev. C **46**, 1094 (1992).
[28] T. Suzuki, D. F. Measday, and J. P. Roalsvig, Phys. Rev. C **35**, 2212 (1987).
[29] M. Gmitrö and P. Truöl, *Advances in Nuclear Physics* (Plenum, New York, 1987), Vol. 18, pp. 241–314.
[30] V. Bobrov, V. Vorlamov, Yu. Grashin, B. Dolgashein, V. Kirillov-Ugryumov, Yu. Nikitin, V. Roganov, A. Saoilov, and S. Somov, Sov. J. Nucl. Phys. **4**, 53 (1967).
[31] R. A. Eramzhyan, V. Kuz'min, and T. Tetereva, JINR Report No. E4-96-478, Dubna, 1996.
[32] D. H. Wright *et al.*, Nucl. Instrum. Methods Phys. Res. A **320**, 249 (1992).
[33] J. P. Perroud *et al.*, Nucl. Phys. **A453**, 542 (1986).
[34] R. Brun, F. Bruyant, M. Maire, A. C. McPherson, and P. Zanarini, GEANT3 (1986), CERN Report No. DD/EE/84-1 (unpublished).
[35] C. W. de Jager, H. de Vries, and C. de Vries, At. Data Nucl. Data Tables **14**, 479 (1974).
[36] *Nuclear Physics and Technology*, edited by H. Schopper (Springer, Berlin, 1967), Vol. 2.
[37] K. W. Ford and J. G. Wills, Nucl. Phys. **35**, 295 (1962).
[38] A. Possoz, D. Favart, L. Grenacs, J. Lehmann, P. Macq, D. Meda, L. Palffy, J. Julien, and C. Samour, Phys. Lett. **50B**, 438 (1974).
[39] L. Ph. Roesch, V. L. Telegdi, P. Truttmann, A. Zehnder, L. Grenacs, and L. Palffy, Phys. Rev. Lett. **46**, 1507 (1981).
[40] Y. Kuno, J. Imazato, K. Nishiyama, K. Nagamine, T. Yamazaki, and T. Minamisono, Phys. Lett. **148B**, 270 (1984); Z. Phys. A **323**, 69 (1986).
[41] M. Morita, R. Morita, and K. Koshigiri, Nucl. Phys. **A577**, 387 (1994).
[42] J. P. Deutsch, L. Grenacs, J. Lehmann, P. Linik, and P. C. Macq, Phys. Lett. **29B**, 66 (1969).
[43] F. B. Kane, M. Eckhause, G. H. Miller, B. L. Roberts, M. E. Vislay, and R. E. Welsh, Phys. Lett. **43B**, 292 (1973).
[44] W. C. Haxton and Calvin Johnson, Phys. Rev. Lett. **65**, 1325 (1990).
[45] T. P. Gorringe, B. Johnson, J. Bauer, M. Kovash, R. Porter, D. S. Armstrong, M. D. Hasinoff, D. F. Measday, B. A. Moftah, and D. H. Wright, Phys. Rev. Lett. **72**, 3472 (1994).
[46] B. Johnson, T. P. Gorringe, J. Bauer, M. Kovash, R. Porter, D. S. Armstrong, M. D. Hasinoff, D. F. Measday, B. A. Moftah, and D. H. Wright, Phys. Rev. C **54**, 2714 (1996).
[47] G. H. Miller, M. Eckhause, F. R. Kane, P. Martin, and R. E. Welsh, Phys. Rev. Lett. **29**, 1194 (1972).
[48] V. Brudanin *et al.*, Nucl. Phys. **A587**, 577 (1995).
[49] B. A. Moftah, E. Gete, D. F. Measday, D. S. Armstrong, J. Bauer, T. P. Gorringe, B. L. Johnson, B. Siebels, and S. Stanislaus, Phys. Lett. B **395**, 157 (1997).